



Power Electronic Systems  
Laboratory

© 2014 IEEE

Proceedings of the International Power Electronics Conference - ECCE Asia (IPEC 2014), Hiroshima, Japan, May 18-21, 2014

## **Low-Complexity Analytical Approximations of Switching Frequency Harmonics of 3-Phase N-Level Voltage-Source PWM Converters**

R. Burkart,  
J.W. Kolar

This material is published in order to provide access to research results of the Power Electronic Systems Laboratory / D-ITET / ETH Zurich. Internal or personal use of this material is permitted. However, permission to reprint/republish this material for advertising or promotional purposes or for creating new collective works for resale or redistribution must be obtained from the copyright holder. By choosing to view this document, you agree to all provisions of the copyright laws protecting it.



Eidgenössische Technische Hochschule Zürich  
Swiss Federal Institute of Technology Zurich

# Low-Complexity Analytical Approximations of Switching Frequency Harmonics of 3-Phase $N$ -Level Voltage-Source PWM Converters

Ralph M. Burkart and Johann W. Kolar  
 Power Electronic Systems Laboratory  
 ETH Zurich, Physikstrasse 3  
 Zurich, 8092, Switzerland  
 burkart@lem.ee.ethz.ch

**Abstract**—In this paper, analytical calculations of the switching frequency harmonics of PWM-controlled 3-phase voltage-source DC/AC power converters are presented. Detailed knowledge of the modulation-dependent spectra of such systems is highly valuable for the EMI filter design and the estimation of the high-frequency losses in the filter components and the load. The paper presents a formula for the calculation of the switching frequency harmonics which is simple and highly versatile. It can be applied to converters with arbitrary numbers of voltage levels  $N$  and in combination with a broad variety of modulation signals. All calculations are verified by means of simulations and show a high accuracy over a wide range of input parameters. Finally, an EMI filter design example demonstrates the practical application and benefits of the derived formula. The MATLAB code used for the calculations is provided at the end of the paper.

## I. INTRODUCTION

Switched-mode pulse-width-modulated (PWM) 3-phase power converters with a voltage-type DC-link are the backbone of a wide range of today's power electronics applications, such as AC motor drive systems, grid-connected converters in renewable energy systems and uninterruptible power supplies (UPS). Besides generating the fundamental voltages which drive the desired fundamental currents, such systems also generate undesired high-frequency (HF) voltage harmonics as an inherent result of the PWM switched-mode operation. These HF harmonics often have a crucial impact on the system design: on the one hand, the harmonic spectrum determines the required EMI filter attenuation in grid-connected applications and for motor drive inverters. On the other hand, the resulting HF currents, i.e. the ripple currents cause additional losses in the filter components and the load (e.g. electrical machines). Consequently, a detailed knowledge of the converter's harmonic spectrum is a basic requirement for the appropriate design of the full converter system. It is furthermore particularly important if accurate efficiency estimations for low-load operation are required where the HF losses usually become increasingly dominant compared to the losses associated with the fundamental current.

A simple approach to compute the switching frequency harmonics of a PWM-controlled converter is by means of applying the fast Fourier transform (FFT) to the respective simulated or measured waveforms. However, the accuracy of the FFT is limited by the number of available sampling points which potentially results in a high computational effort [1]. As a consequence, the use of versatile yet simple analytical

methods can offer advantages if a systematic insight regarding the spectra of different converter topologies, modulation signals and modulation depths must be gained.

A wide variety of methods exist to analytically describe the harmonics of PWM signals. While decomposition techniques [2], implicit descriptions [3] and Kapteyn [4] or Lagrange [5] series have been reported, by far the most widely used method in literature is the double-Fourier-series (DFS) analysis based on 3D geometric wall-model representations of the PWM signal. The method was originally presented in [6] and [7] and later adopted for different 3-phase current- and voltage-source PWM converters employing various PWM schemes. [1], [8]–[12]. An extensive overview of the formulas obtained from this method can be found in [13].

The above mentioned methods have the common benefit of yielding exact analytical closed-form results. The main drawback, however, lies in the requirement of deriving new formulas for each combination of topology and type of modulation signal. These derivations and the results are involved and the mathematical effort increases quickly with increasing number of voltage levels and more demanding modulation signals. Generalized formulas exist either for  $N$ -level converters with restriction to a pure sinusoidal modulation signal [10], [13], or for converters with 2-level characteristics only but arbitrary modulation signals [1]. These results are even more intricate and cannot readily be applied. Eventually, all methods generate formulas including infinite double sums of Bessel functions which considerably impedes the numerical evaluation.

An alternative but not widely used approach for the analytical calculation of switching frequency harmonics is presented in [14]. This method is based on a subsequent local and global integration and is thus called local-global-integral (LGI) method for the remainder of this work. The LGI method overcomes most of the above stated drawbacks. In particular, the resulting formula can take into account a broad variety of modulation signals and consists of a simple integral which is numerically easy to evaluate. However, the LGI method assumes an infinitely high number  $z$  of switching intervals within a period of the output voltage fundamental and is thus, in contrast to most other methods, not exact in the case of real converter systems with finite switching frequencies. Nevertheless, sufficient accuracy can still be obtained in most practical cases, i.e. for converters with  $z \geq 30$ .

The LGI method has so far only been applied to a 2-level

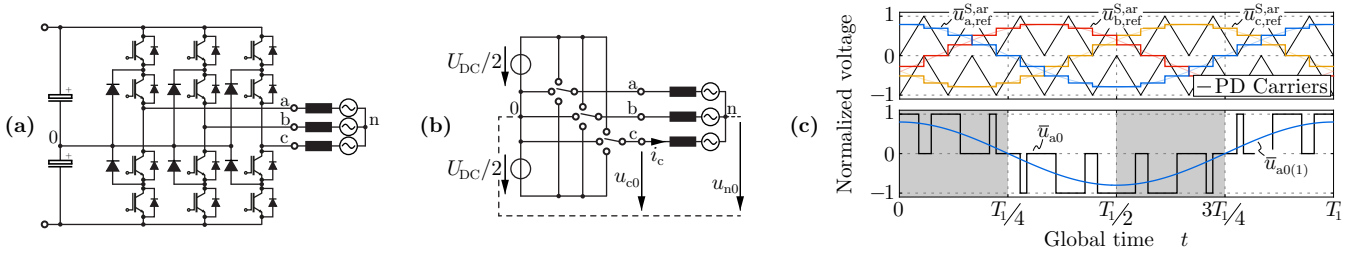


**Fig. 1:** 3-phase 3-level voltage-source DC/AC power converter with sinusoidal PWM. **(a)** Typical practical implementation. **(b)** Idealized model used for the harmonic analysis in this work. **(c)** Asymmetric regular-sampling PWM with synchronized phase disposition (PD) carrier waves, sampled sinusoidal reference signals  $\bar{u}_{p,\text{ref}}^{\text{S,ar}}$ ,  $p = \{a,b,c\}$  and resulting idealized output voltage pattern  $\bar{u}_{a0}$  and fundamental harmonic  $\bar{u}_{a0(1)}$ . Due to the underlying assumptions in this work, the converter output voltages feature a quarter-wave symmetry, i.e.  $\bar{u}_{p0}(t) = \bar{u}_{p0}(-t) = -\bar{u}_{p0}(t + T_1/2)$ .

converter in [14]. Moreover, a detailed analysis of the accuracy and limitations of the result is missing yet. In this paper, it is shown that the LGI method can also be applied to a 3-level converter with only moderate mathematical effort and yielding a similarly simple formula with high accuracy (**Sec. II**). In a second step, the LGI method is used to derive an advanced but still simple and versatile universal formula which describes the voltage and current harmonics of a general  $N$ -level converter with almost arbitrary modulation signal. Finally, an example of application is given which demonstrates how the formula can be used to design an EMI filter (**Sec. IV**). The **Appendix** contains the MATLAB implementation of the general  $N$ -level converter formula derived in this work.

## II. LGI METHOD FOR 3-LEVEL CONVERTERS

In this section, the LGI method presented in [14] is adopted for a 3-level 3-phase voltage-source converter as shown in **Fig. 1(a)**. **Sec. II-A** gives a short overview of possible PWM schemes for this topology. After discussing the underlying assumptions in **Sec. II-B**, the derivation of the formula to calculate the switching frequency voltage harmonics is presented in **Sec. II-C** and **Sec. II-D**. **Sec. II-E** compares the obtained LGI-based result to the existing DFS-based result and **Sec. II-F** presents a verification of the derived formula and investigates its accuracy and the useful parameter ranges.

For the remainder of this work,  $T_1 = 1/f_1$  denotes the fundamental period and  $T_{\text{sw}} = 1/f_{\text{sw}}$  the switching period. Where a distinction between the two different periods is necessary, the position within  $T_1$  is described by the (macroscopic) global time  $t$  while the (microscopic) local time  $t_\mu$  is used to refer to the position within a switching interval  $[-T_{\text{sw}}/2, T_{\text{sw}}/2]$ , placed symmetrically around  $t$ . Normalized voltages are denoted by overlines,  $\bar{u} = u/(U_{\text{DC}}/2)$ .  $p$  stands for one of the three phases  $\{a,b,c\}$  with corresponding phase shifts  $\phi = \{0, -2\pi/3, 2\pi/3\}$ .  $u_{p,\text{ref}}$  denotes an arbitrary modulation signal while  $u_{p,\text{ref}}^*$  is a specific modulation signal, e.g.  $u_{p,\text{ref}}^{\text{S}}$  denoting a pure sinusoidal signal. The term “reference signal” is equivalently used for “modulation signal”.

### A. PWM Schemes for 3-Level Converters

In this section, PWM schemes employing different carrier signals and sampling techniques are discussed, while the discussion of different modulation signals follows in **Sec. II-D**.

The most basic idea of PWM employed in DC/AC power converters is to generate trains of rectangular switched voltage pulses  $u_{p0}$  whose fundamental  $u_{p0(1)}(t)$  is equal to a given sinusoidal modulation signal, i.e. the reference signal  $u_{p,\text{ref}}^{\text{S}}$  (cf. **Fig. 1**),

$$u_{p0(1)}(t) \equiv u_{p,\text{ref}}^{\text{S}}(t) \equiv \hat{U}_{\text{ref}} \cos[2\pi f_1 t + \phi]. \quad (1)$$

This can be achieved by determining the switching instants through intersection of the reference signal with a HF carrier signal as depicted in **Fig. 2**. Commonly used carriers are periodic sawtooth or triangular signals. However, only triangular carriers are considered here since sawtooth carriers generally lead to a higher harmonic distortion of the generated output  $u_{p0}$  [13]. For a 3-level topology, 2 carriers are required which can be implemented with either phase disposition (PD) or phase opposition disposition (POD) as shown in **Fig. 2(a)**. This work focuses on PD carriers rather than POD carriers due to the better harmonic performance that can be achieved in three-phase systems [10], [13]. Finally, using a digitally sampled reference curve  $\bar{u}_{p,\text{ref}}^{\text{ar}}$  (asymmetric regular sampling PWM) rather than a continuous signal  $\bar{u}_{p,\text{ref}}^{\text{n}}$  (natural sampling PWM) is better suited for the digital controllers employed in most modern converters. Regular sampling PWM generates slightly different voltage pulses (and thus different harmonic amplitudes) when compared to natural sampling PWM as depicted in **Fig. 2(b)**. The switching rules, however, are independent from the type of sampling or the reference signal waveform,

$$\bar{u}_{p0}(t) = \begin{cases} 1 & \bar{u}_{p,\text{ref}}(t) \geq \text{carrier}_{\text{high}}(t) \\ 0 & \text{carrier}_{\text{low}}(t) \leq \bar{u}_{p,\text{ref}}(t) < \text{carrier}_{\text{high}}(t) \\ -1 & \bar{u}_{p,\text{ref}}(t) < \text{carrier}_{\text{low}}(t) \end{cases}. \quad (2)$$

Whether natural or asymmetric regular sampling is used becomes irrelevant at very high switching frequency ratios  $z$  due to the vanishing differences between the generated voltage pulses and switching instants. As high values of  $z$  are assumed for all analytical calculations throughout this work, the sampling type is not indicated anymore for the remainder of this paper. For all simulations used to evaluate the calculated results, a PWM scheme with PD carriers and regular sampling is employed (**Fig. 1(c)**).

A typical spectrum of the output voltages  $u_{p0}$ , employing the selected PWM scheme with triangular PD carriers, can be seen in **Fig. 3**. The spectrum contains harmonic groups at integer multiples  $m$  of the carrier frequency  $f_{\text{sw}}$ . Within these groups, the individual harmonics are integer multiples  $k$  of the fundamental frequency  $f_1$  distant from each other. Based on this observation, the harmonic order  $q$  of a particular harmonic  $\hat{U}_{p0(q)}$  can uniquely be expressed by

$$q = mz + k, \quad m \in \mathbb{N}, k \in \mathbb{Z} \mid |k| \leq \lfloor z/2 \rfloor, \quad (3)$$

where  $\lfloor * \rfloor$  denotes the floor function.

General remark: although this work is based on the consideration of triangle-carrier-based PWM, the presented analysis is also valid for space-vector-based modulation concepts. This is due to the existence of equivalent reference signals in a triangle-carrier-based PWM scheme which can be used to represent any space-vector modulation scheme [15].

### B. Assumptions

In order to successfully apply the LGI method, the following assumptions must be made:

- (i) The converter output PWM phase voltages  $u_{p0}(t)$  are ideal rectangular, even and periodical with  $T_1$ ,

$$u_{p0}(t) = u_{p0}(-t) = u_{p0}(t \pm nT_1), \quad n \in \mathbb{N}_0. \quad (4)$$

- (ii) The ratio  $z$  between switching frequency  $f_{sw}$  and fundamental frequency  $f_1$  is assumed to be very high, i.e. theoretically tending towards infinity,

$$z = \frac{f_{sw}}{f_1} \rightarrow \infty. \quad (5)$$

- (iii) The frequency ratio  $z$  is odd and a multiple value of 3,

$$z = 6n + 3, \quad n \in \mathbb{N}_0. \quad (6)$$

Assumption (i) implies the consideration of a converter with idealized switches and a constant DC-link voltage source  $U_{DC}$  as depicted in **Fig. 1(b)**. Assumption (ii) is required for the mathematical derivations. In practice, however, for the considered asymmetric regular sampling  $z \geq 30$  is sufficient to achieve accurate results (see **Sec. II-F**, [14]). The presented formula in this work can in theory be applied for arbitrary values of  $z \geq 30$ . However, an odd frequency ratio is assumed in (iii) as this guarantees odd harmonics only and avoids a DC offset of the output phase voltages (cf. **Fig. 3**). Even harmonics and DC offsets are generally undesired in practice, which is also reflected by the more stringent limits for such harmonics in grid harmonics standards such as [16]–[18]. The restriction to multiples of 3 in (iii) allows for synchronized, symmetric PWM of the three phases  $\{a,b,c\}$  with the same PD carrier signals for all references (cf. **Fig. 1(c)**). Assumption (iii) in conjunction with (i) furthermore implies output signals with quarter-wave symmetry (cf. **Fig. 1(c)**) and associated spectra that contain odd order cosine terms only,

$$u_{p0}(t) = \sum \hat{U}_{p0(q)} \cos[q(2\pi f_1 t + \phi)], \quad q=2n+1, \quad n \in \mathbb{N}_0. \quad (7)$$

Note that due to the symmetric PWM the amplitudes  $\hat{U}_{p0(q)}$  are identical in all three phases. Furthermore, there are no phase shifts other than  $\pm\pi$  between the harmonics of the individual phases which is taken into account by negative harmonic amplitudes  $\hat{U}_{p0(q)}$ . Finally, the consideration of only even output signals  $u_{p0}$  does not represent a restriction in practice as it can always be achieved by appropriately defining the coordinates.

### C. Analytical Derivations

In a first step of the LGI method, a local Fourier analysis within a single switching period is performed. This result can later be used for a global analysis of the full fundamental period. For reasons of symmetry (assumption (iii)), it is sufficient to perform the analysis for phase  $p = a$  only.

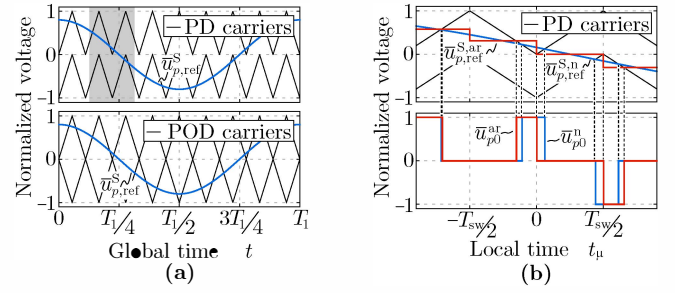


**Fig. 2:** PWM schemes for 3-level converters. (a) HF triangular carriers with phase disposition (PD) and phase opposition disposition (POD), sinusoidal reference signal  $\bar{u}_{p,\text{ref}}^S$ . (b) Detail of (a) (marked gray) showing the generation of the switching time instants by intersection of the reference signal with the HF PD carriers. The digitally sampled reference  $\bar{u}_{p,\text{ref}}^{S,\text{ar}}$  used for asymmetric regular sampling PWM results in slightly different voltage pulses than the continuous reference  $\bar{u}_{p,\text{ref}}^{S,n}$  used for natural sampling PWM.

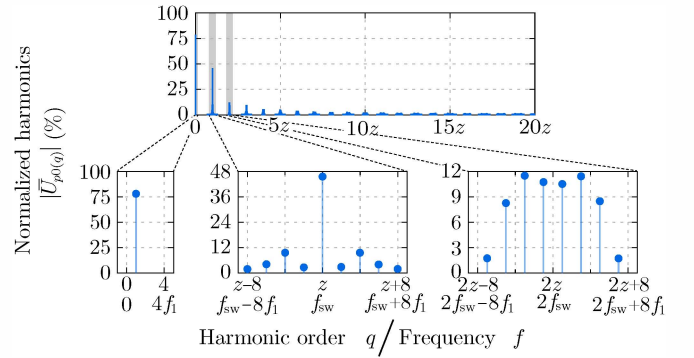


**Fig. 3:** Typical spectrum of the output voltages  $\bar{u}_{p0}$  for high frequency ratios  $z$  and a PWM scheme with triangular PD carriers. The spectrum contains baseband low-frequency (LF) harmonics and harmonic groups centered around integer multiples  $m$  of the carrier frequency, i.e. the switching frequency  $f_{sw}$ . For high values of  $z$ , the baseband harmonics represent the harmonic content of the used reference signal (here pure sinusoidal reference  $\bar{u}_{p,\text{ref}}^S$  and thus one harmonic at the fundamental frequency  $f_1$ ). Within the harmonic groups at integer multiples  $m$  of  $f_{sw}$ , sideband harmonics occur at integer multiples  $k$  of the fundamental frequency  $f_1$  distant from the respective center frequency  $m f_{sw} = m z f_1$ . Thus, for  $z = \frac{f_{sw}}{f_1}$ , the harmonic order  $q = m z + k$  can be defined with reference to  $f_1$ . As a result of the considered triangular PD carriers only sidebands with  $k$  even around odd  $m$  and with  $k$  odd around even  $m$  occur. Consequently, if  $z$  is odd, only odd order harmonics occur.

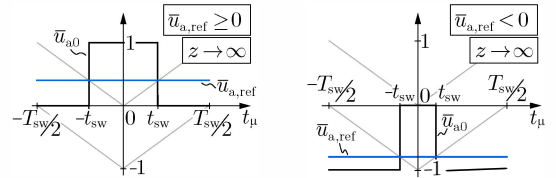


**Fig. 4:** Normalized output voltage pattern  $\bar{u}_{a0}(t_\mu)$  within a single switching period  $T_{sw}$  depending on the sign of the reference signal  $u_{a,\text{ref}}(t)$ . Due to the assumed infinite switching frequency ratio  $z$ , the considered time interval is very short and thus the reference signal does not change,  $\bar{u}_{a,\text{ref}}(t) = \text{const.}$  for  $t_\mu \in [-T_{sw}/2, T_{sw}/2]$ . As a consequence, the switching instants are symmetric around  $t_\mu = 0$  and  $\bar{u}_{a0}(t_\mu) = \bar{u}_{a0}(-t_\mu)$ .

1) *Local Analysis:* The voltage pattern within a single switching period can be seen in **Fig. 4**. Due to assumption (ii),  $z \rightarrow \infty$ , the reference value  $\bar{u}_{a,\text{ref}}$  is constant within the infinitely short switching period. As a result, the output voltage  $\bar{u}_{a0}$  is symmetric around  $t_\mu = 0$  with the switching times

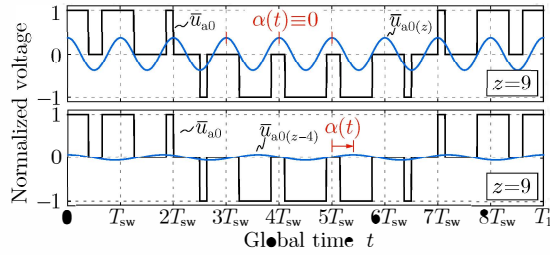


**Fig. 5:** Normalized output voltage  $\bar{u}_{a0}(t)$  and its 9<sup>th</sup> and 5<sup>th</sup> harmonic  $\bar{u}_{a0(9)}(t)$  and  $\bar{u}_{a0(5)}(t)$ , respectively, for  $z=9$ . While the carrier harmonics at integer multiples of  $z$  ( $q=mz$ ) stay in phase with respect to the consecutive switching periods, the sideband harmonics with  $q=mz+k$ ,  $k \neq 0$ , experience a phase shift  $\alpha(t)$ . The low frequency ratio  $z=9 < 30$  has been chosen for the purpose of a clearer illustration.

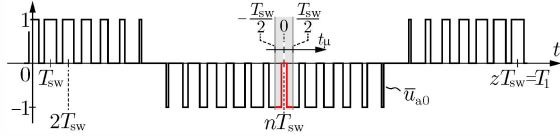


**Fig. 6:** Summation (13) of the  $z$  local Fourier integrals (12) at the positions  $t=nT_{sw}$ ,  $n = \{1, \dots, z\}$ , over the fundamental period  $T_1 = zT_{sw}$ . For  $z \rightarrow \infty$ ,  $T_{sw} \rightarrow dt$ , and  $nT_{sw} \rightarrow t$ . As consequence, the sum (13) can be expressed as the integral (16).

$$|t_{sw}(t)| = \begin{cases} \frac{T_{sw}}{2} \bar{u}_{a,ref}(t) & \bar{u}_{a,ref}(t) \geq 0 \\ \frac{T_{sw}}{2} (1 + \bar{u}_{a,ref}(t)) & \bar{u}_{a,ref}(t) < 0 \end{cases} \quad (8)$$

The local Fourier analysis within a single switching period over the local time  $t_\mu$  can now be carried out using

$$\hat{U}_{a0(q)}[t] = \frac{U_{DC}}{T_{sw}} \int_{-\frac{T_{sw}}{2}}^{\frac{T_{sw}}{2}} \bar{u}_{a0}(t, t_\mu) \cos[q2\pi f_1 t_\mu - \alpha(t)] dt_\mu \quad (9)$$

Although the periods  $T_q = T_{mz+k}$  with  $k \neq 0$  of the sideband harmonics do not equal integer multiples of the switching period  $T_{sw}$ , the difference becomes negligibly small for  $z \rightarrow \infty$  and finite  $k$ ,

$$qf_1 = (mz+k)f_1 \stackrel{z \gg k}{\approx} mzf_1 = \frac{m}{T_{sw}}, \quad (10)$$

and hence (9) can be used without restrictions for both the carrier harmonics ( $k=0$ ) and the sideband harmonics ( $k \neq 0$ ). Note that finite values of  $k$  are guaranteed by definition (3) of  $q$ , where  $|k|$  is minimized with respect to  $mz$  which consequently also minimizes the approximation error in (10).

Over the course of the fundamental period, the sideband harmonics experience a phase shift  $\alpha(t)$  with respect to the individual switching periods,

$$\alpha(t) = k2\pi f_1 t \quad (11)$$

This phase shift is illustrated in **Fig. 5** for the case of a carrier harmonic at a multiple of the switching frequency ( $k=0$ ) where the phase shift is always zero and for a sideband harmonic ( $k \neq 0$ ) with non-zero phase shift.

Using (8), (10) and (11), the integral (9) can be solved,

$$\hat{U}_{a0(q)}[t] = \frac{U_{DC}}{m\pi} \cos[k2\pi f_1 t] \sin[m\pi \bar{u}_{a,ref}(t)] \cdot \begin{cases} 1 & \bar{u}_{a,ref}(t) \geq 0 \\ (-1)^m & \bar{u}_{a,ref}(t) < 0 \end{cases} \quad (12)$$

2) *Global Analysis:* In order to obtain the global harmonics  $\hat{U}_{a0(q)}$  of the entire fundamental period  $T_1 = zT_{sw}$ , i.e. the actual output voltage spectrum, the local results (12) of the  $z$  individual switching intervals must be summed up and weighted accordingly (cf. **Fig. 6**),

$$\hat{U}_{a0(q)} = \frac{1}{zT_{sw}} \sum_{n=1}^z \hat{U}_{a0(q)}[nT_{sw}] \cdot T_{sw} \quad (13)$$

For an infinite switching frequency ratio  $z \rightarrow \infty$ ,

$$\frac{T_1}{z} = T_{sw} \xrightarrow{z \rightarrow \infty} dt, \quad (14)$$

$$n \frac{T_1}{z} = nT_{sw} \xrightarrow{z \rightarrow \infty} t, \quad (15)$$

the local time interval  $T_{sw}$  is converted into a global time differential  $dt$  and the discrete points of time  $nT_{sw}$  merge into the continuous global time  $t$ . As a consequence, the sum in (13) can be expressed as a global integral,

$$\hat{U}_{a0(q)} \stackrel{z \rightarrow \infty}{=} \frac{1}{T_1} \int_0^{T_1} \hat{U}_{a0(q)}[t] dt \quad (16)$$

The above integral (16) again illustrates how the contributions of the individual switching periods for a specific harmonic are averaged over the fundamental period. This local-global integral method (LGI) assuming infinite switching frequency ratios  $z$  can also be found in [19], [20] for the calculation of the semiconductor currents of PWM converters. Substitution of  $\hat{U}_{a0(q)}[t]$  in (16) with (12) yields,

$$\hat{U}_{a0(q)} = \frac{2[1 - (-1)^{m+k}] U_{DC}}{m\pi T_1} \cdot \int_0^{\frac{T_1}{4}} \cos[k2\pi f_1 t] \sin[m\pi \bar{u}_{a,ref}(t)] dt, \quad (17)$$

where the quarter-wave symmetry of  $\bar{u}_{a0}$  was exploited.

3) *Final Result:* Eq. (17) can be further simplified as it does not depend on  $T_1$ . In order to see this, the substitution

$$\beta = 2\pi f_1 t, \quad (18)$$

is used to obtain the final result

$$\hat{U}_{a0(q)} = \frac{[1 - (-1)^{m+k}] U_{DC}}{m\pi^2} \cdot \int_0^{\frac{\pi}{2}} \cos[k\beta] \sin[m\pi \bar{u}_{a,ref}(\beta)] d\beta,$$

$$q = mz + k, \quad m \in \mathbb{N}, \quad k \in \mathbb{Z} \mid |k| \leq \lfloor z/2 \rfloor, \quad (19)$$

where  $\bar{u}_{a,ref}(\beta)$  is the reference signal  $\bar{u}_{a,ref}(t)$  with its period normalized to  $2\pi$ . Inspection of (19) results in the following observations:

- The effective amplitude of a particular harmonic with order  $q$  is the result of (infinite) overlapping sidebands. E.g. for  $z = 33$ , both  $(m, k) = (1, 2)$  and  $(m, k) = (2, -31)$  contribute to the harmonic at  $q = 35$ .
- For continuous and bounded reference signals  $\bar{u}_{a,ref}(t)$ , the integral in (19) yields decreasing values for increasing ratios  $|k|/m$ . Moreover, the values become less accurate due to approximation (10).
- By means of the unique definition (3) of  $q$  which minimizes  $|k|$  with respect to  $mz$ , only the most significant and

most accurate sideband contribution  $(m, z)$  is considered in (19).

- Note again that only the amplitudes of the harmonics are approximated in (19) whereas the resulting phase shifts (0 or  $\pm\pi$ ) are exact.

Further mathematical conversions of (19), i.e. the analytical evaluation of the integral is only possible with a given reference and would lead to more complex expressions containing Bessel functions as known from [8]–[10]. Instead, direct numerical integration is preferred as shown in the next section.

#### D. Evaluation for Different Reference Signals

Eq. (19) is the result in its most general form which can easily be evaluated numerically for almost any given reference  $\bar{u}_{a,\text{ref}}$ . Assumptions (i) and (iii) imply the class of permissible reference signals  $\bar{u}_{p,\text{ref}}$  that generate output voltage waveforms  $u_{p0}$  with the assumed properties. Any even reference signal consisting of only odd order cosine terms is possible,

$$\bar{u}_{p,\text{ref}}(\beta) = \sum \hat{U}_{\text{ref}(q)} \cos[q(\beta + \phi)], \quad q=2n+1, \quad n \in \mathbb{N}_0. \quad (20)$$

All permissible reference signals feature quarter-wave symmetry. Besides the standard pure sinusoidal reference,

$$\bar{u}_{p,\text{ref}}^{\text{S}}(\beta) = M \cos[\beta + \phi], \quad (21)$$

with  $M = \frac{U_{p0(1)}}{U_{\text{DC}/2}}$  being the modulation depth, other common and widely applied references belong to this class. Examples are the sinusoidal PWM with third harmonic injection,

$$\bar{u}_{p,\text{ref}}^{\text{S3}}(\beta) = M(\cos[\beta + \phi] - \frac{1}{6} \cos[3\beta]), \quad (22)$$

or the symmetric PWM,

$$\bar{u}_{p,\text{ref}}^{\text{SY}}(\beta) = \begin{cases} \frac{\sqrt{3}}{2} M \cos[\beta - \frac{\pi}{6} + \phi] & 0 \leq \beta < \frac{\pi}{3} \\ \frac{3}{2} M \cos[\beta + \phi] & \frac{\pi}{3} \leq \beta < \frac{\pi}{2} \end{cases}, \quad (23)$$

which allow for an increased linear range of the modulation depth ( $M_{\text{max}} = 2/\sqrt{3}$  instead of  $M_{\text{max}} = 1$  for pure sinusoidal PWM). The 60° flat-top PWM,

$$\bar{u}_{p,\text{ref}}^{\text{FT}}(\beta) = \begin{cases} 1 & 0 \leq \beta < \frac{\pi}{6} \\ -1 + \sqrt{3} M \cos[\beta - \frac{\pi}{6} + \phi] & \frac{\pi}{6} \leq \beta < \frac{\pi}{2} \end{cases}. \quad (24)$$

can be employed to additionally decrease the switching losses at the expense of a richer harmonic spectrum. Further information on the above types of reference signals can be found in [15].

Eq. (19) can now be evaluated when substituting  $\bar{u}_{a,\text{ref}}$  by a concrete reference signal, e.g. the pure sinusoidal reference. E.g. for  $q = 1 \cdot z + 4$ ,  $M = 0.8$  we obtain (cf. **Fig. 3**),

$$\begin{aligned} \hat{U}_{a0(1+z+2)} &= \frac{2U_{\text{DC}}}{\pi^2} \int_0^{\frac{\pi}{2}} \cos[2\beta] \sin[1 \cdot \pi \cdot 0.8 \cdot \cos[\beta]] d\beta \\ &\approx -0.093 \frac{U_{\text{DC}}}{2}. \end{aligned} \quad (25)$$

#### E. Comparison to the Double-Fourier-Series Method

Applying the widely used double-Fourier-series (DFS) method instead of the LGI method used in this work, the following formula for the calculation of the switching frequency harmonics  $\hat{U}_{a0(q)}^{\text{DFS}}$  of a 3-level converter employing PD carriers and natural sampling can be obtained [13],

$$\begin{aligned} \hat{U}_{a0(q)}^{\text{DFS}} &= \sum_{\substack{mz+k=q \\ m \in \mathbb{N}, k \in \mathbb{Z}}} \frac{U_{\text{DC}}}{m\pi} (1 - \cos[(m+k)\pi]) \\ &\cdot \left[ \begin{aligned} &J_k[m\pi M] \sin[k\frac{\pi}{2}] \\ &+ \frac{4}{\pi} \sum_{\substack{n=1 \\ 2n-1 \neq |k|}}^{\infty} J_{2n-1}[m\pi M] \frac{(2n-1) \cos[k\frac{\pi}{2}]}{(2n-1+k)(2n-1-k)} \end{aligned} \right]. \end{aligned} \quad (26)$$

Note that an appropriate formula for asymmetric regular sampling could not be found in the literature. By inspection of (26) several observations can be made:

- Formula (26) is clearly more complex than the LGI-method-based formula (19). Furthermore, in contrast to (19), (26) is only valid for a pure sinusoidal reference signal and different formulas would thus be required in case of other references.
- The result (26) is exact in theory. However, the numerical evaluation is involved due to the present Bessel functions and infinite sums. Especially the latter can only be approximated in practice. Therefore, on the one hand, the DFS method does not yield exact results in practice and on the other hand, a careful error analysis is required as for the LGI method (cf. **Sec. II-F**).
- A fundamental difference between the DFS-based and the LGI-based result lies in the first summation in (26). This summation takes into account the overlapping sideband contributions of all possible combinations  $(m, z)$ ,  $m \in \mathbb{N}, k \in \mathbb{Z}$  with  $mz + k = q$ . In contrast, the LGI-based formula (19) neglects this summation as this results in only small errors if large  $z$  are assumed.

In [13], a simplified and more flexible result of the DFS method is presented for 2-level converters. It contains, similar to the LGI-based result presented in this paper, an unevaluated integral instead of Bessel functions and can be used for several reference signals. However, no such result is presented for 3-level and  $N$ -level converters and the complexity of the corresponding derivation and possible result remains unclear.

#### F. Verification and Error Analysis

**Fig. 7** compares the significant, i.e. dominant harmonics occurring at the switching frequency multiples  $m = \{1, 5, 15\}$ , calculated by means of (19) and by means of a simulation-based FFT for the flat-top PWM (24) and  $z = 243$ . The figure proofs the validity of the formula and that a high accuracy can be obtained.

A systematic and detailed analysis of the achievable accuracy of the presented formula was performed. However, due to reasons of brevity, only the results of this analysis can be presented here.

In a first step, a lower limit  $z = z_{\text{min}}$  was searched for which assumption (ii),  $z \rightarrow \infty$ , is sufficiently met yielding high accuracy of the calculated harmonics. As for 2-level systems [14], it was found that

$$z \geq z_{\min} = 30, \quad (27)$$

is sufficient yielding amplitude errors below 10%.

By inspection of **Fig. 7**, it can be observed that the errors tend to increase with increasing harmonic order. A detailed analysis reveals that the total energy of the calculated harmonics decreases when compared to the FFT-based harmonics as the occurring overlapping at high frequencies is not taken into account (cf. **Sec. II-E**). Therefore, in a second step, it was investigated up to what harmonic orders the result still provides sufficient accuracy. It was found that the maximum permissible value of  $m$  increases for higher values of  $z$ . If the energy deviation between each calculated harmonic group to the corresponding FFT-based results is limited to  $< 20\%$ , the upper limit for  $m$ ,

$$m_{\max}(z) = \begin{cases} z/5 & \bar{u}_{p,\text{ref}} \in \{\bar{u}_{p,\text{ref}}^S, \bar{u}_{p,\text{ref}}^{S3}\} \\ z/6 & \bar{u}_{p,\text{ref}} \in \{\bar{u}_{p,\text{ref}}^{SY}, \bar{u}_{p,\text{ref}}^{\text{FT}}\} \end{cases}, \quad (28)$$

can be found.

Based on the above analysis it can thus be concluded that the obtained formula can be applied to most modern 50/60 Hz grid-connected converters which normally readily fulfill  $z \geq z_{\min}$  ( $f_{\text{sw}} \geq 1.5/1.8 \text{ kHz}$ ). Moreover, the defined upper bound in this section mostly represents no serious practical constraint for the application of the result of this paper, as in many applications only the dominant low-order harmonics are of interest.

### III. GENERALIZATION FOR $N$ -LEVEL CONVERTERS

The derivations for the 3-level converter shown in **Sec. II** can be generalized with little effort to obtain a universal formula for  $N$ -level topologies as depicted in **Fig. 8(a)**. Since the approach and ideas of the derivation are similar to those already shown, for reasons of brevity only the result is presented here,

$$\hat{U}_{a0(q)} = \frac{2[1 - (-1)^{m+k}]U_{\text{DC}}}{(N-1)m\pi^2} \int_0^{\frac{\pi}{2}} \cos[k\beta] \cdot \sin\left[\frac{m\pi}{2}\left(1 + N - 2N^*[N, \bar{u}_{a,\text{ref}}(\beta)] + (N-1)\bar{u}_{a,\text{ref}}(\beta)\right)\right] d\beta. \quad (29)$$

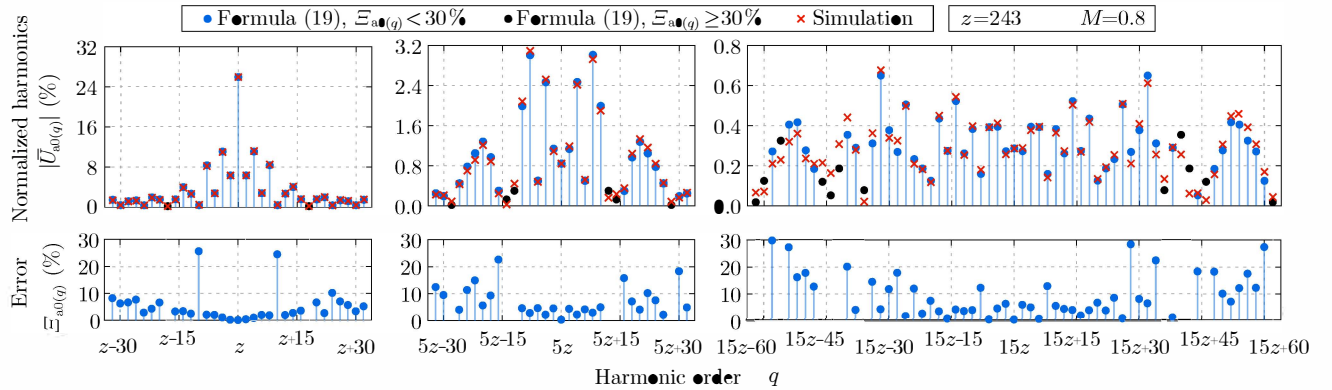


**Fig. 7:** Verification of (19) for the flat-top PWM (24) by means of a comparison to a simulation-based FFT analysis. It can be observed that at higher multiples  $m$  of the switching frequency the growing number of significant sideband harmonics have a lower amplitude but are more widely distributed around the respective center order harmonic at  $q = mz$ . A high accuracy is achieved in general while large individual errors  $\Xi_{a0(q)} > 30\%$  predominantly occur at only non-significant harmonics (marked black). It can be observed, that for increasing harmonic orders the individual errors tend to increase. This is a result of the harmonic groups which start to overlap on the edges at high values of  $m$ . As indicated in (28), the process of overlapping occurs already at lower values of  $m$  if  $z$  is low, as the harmonic groups are located closer to each other than for high values of  $m$ .

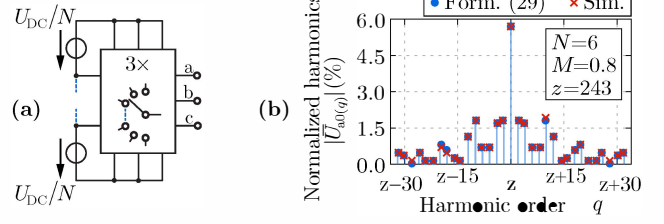


**Fig. 8:** Calculation of the output voltage spectrum of  $N$ -level topologies. (a) General three-phase  $N$ -level voltage source converter. (b) Comparison of the calculated spectra of a 6-level converter using the proposed universal formula (29) and FFT-based values from a simulation.

The function

$$N^*[N, \bar{u}] = 1 + \left\lfloor \frac{(1 + \bar{u})(N-1)}{2} \right\rfloor, \quad (30)$$

identifies the relevant carrier signal  $N^*$  amongst the  $(N-1)$  available PD carriers (cf. **Fig. 2(a)**) as a function of the local value of the reference voltage  $\bar{u}_{a,\text{ref}}(\beta)$ . Formula (29) represents a highly versatile result which can be evaluated for both arbitrary number of voltage levels as well as all reference signals defined in (20). The formula is verified by the example shown in **Fig. 8(b)**.

### IV. EXAMPLE OF APPLICATION

In this section, it is demonstrated how to use the derived formulas in a practical EMI filter design example. **Fig. 9** shows a typical 10 kW solar inverter used in residential applications connected to the public mains. All specifications are listed in **Tab. I**. The input DC/DC boost converter ensures a stable DC-link voltage of  $U_{\text{DC}} = 650 \text{ V}$  which implies a constant modulation depth of  $M = 1.0$  if a constant grid line-voltage of  $\hat{U}_g = (230 \cdot \sqrt{2}) \text{ V}$  is assumed.

Depending on the geographic location, different standards concerning EMI must be fulfilled. For residential solar applications in European countries, IEC 61000-6-3 [21] is a typical standard which ultimately requires compliance with the Class B quasi-peak (QP) EMI limits as stated in CISPR 14 [22]. As a consequence, the output filter of the inverter must be accordingly dimensioned. For simplicity reasons, only the DM

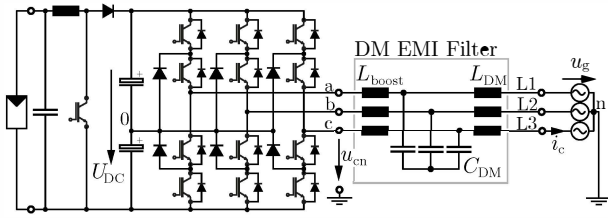


**Fig. 9:** Typical solar inverter connected to the grounded public mains. The DM EMI filter together with the CM filter (not shown) must be designed so as to fulfill EMI limits such as CISPR 14, Class B. The specifications of this converter are listed in **Tab. I**.

**Tab. I:** Specifications of the example solar inverter depicted in **Fig. 9**.

General	Rated power	$P_r$	10 kW
	DC-link voltage	$U_{DC}$	650 V
	Grid line-voltage	$\hat{U}_g$	$(230 \cdot \sqrt{2})$ V
	Grid frequency	$f_g = f_1$	50 Hz
Modulation	Modulation signal	$u_{p,ref}(\beta)$	$u_{p,ref}^S(\beta)$
	Modulation depth	$M$	1.0
	Switching frequency	$f_{sw}$	12.15 kHz
	Frequency ratio	$z$	243
DM filter	EMI standard	IEC 61000-6-3 (CISPR 14, Class B)	
	Boost inductance	$L_{boost}$	300 $\mu$ H
	DM inductance	$L_{DM}$	30 $\mu$ H
	DM capacitance	$C_{DM}$	65 $\mu$ F

filter is designed here, while in reality additional CM filter components must be employed to attenuate the CM emissions.

According to CISPR 16 [23], the QP EMI noise level of a signal must be determined by means of the following procedure:

- 1.) Filtering of the signal with a bandpass filter (RBW filter) with 9 kHz ( $= 2 \cdot 90 \cdot f_1$ ) window width and a filter center frequency of 150 kHz.
- 2.) Application of the obtained filtered signal  $u_{RBW}$  to the predefined QP detector circuit as depicted in **Fig. 10(a)** which provides the steady-state QP emission level  $u_{QP}$  at the output.
- 3.) Sweep of the RBW filter center frequency from 150 kHz to 30 MHz and continuous repetition of steps 1.) and 2.) to obtain the frequency-dependent QP emissions  $u_{QP}(f)$ .

If a calculation of the EMI emissions is preferred over using an actual hardware prototype and appropriate measurement equipment, either a simulation or, more flexibly, the formulas derived in this paper can be used. For the given application

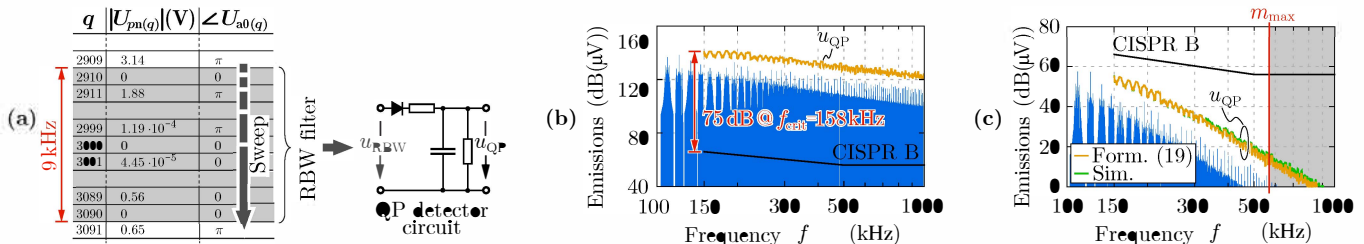


**Fig. 10:** Analysis and design steps of the DM EMI filter of the application shown in **Fig. 9**. (a) Calculation of the quasi-peak (QP) emission levels at the converter output ports {a,b,c}. The calculated DM harmonics ( $q \neq 3n$ ) within the bandpass RBW filter with window width of 9 kHz are used to synthesize the filtered signal  $u_{RBW}$  in time domain, which can then be applied to the QP detector circuit with defined charge and discharge constants. The resulting steady-state voltage across the capacitor is the measured QP emission level  $u_{QP}$ . This procedure is repeated while sweeping the center frequency of the RBW filter from 150 kHz ( $\hat{=} q=3000$ ) to 30 MHz. (b) Calculated spectrum of (a), determined DM emission levels  $u_{QP}$  and permissible QP emission levels according to CISPR 14, Class B [22]. A minimum damping of 75 dB must be achieved at the critical frequency  $f_{crit}=158$  kHz. (c) Calculated emissions including the filter at the ports {L1,L2,L3} and comparison to the emission values obtained with the FFT-based spectrum from a simulation. The error remains lower than 2 dB up to the upper limit  $m_{max}=48 \hat{=} 583$  kHz as defined in **Sec. II-F** and reaches 3 dB at 1 MHz ( $\hat{=} m \approx 82$ ).

in **Fig. 9**, formula (19) was used to create a table of the harmonics of the output voltages  $u_{pn}$  as shown in **Fig. 10(a)**. The described filtering process of step 1.) was then performed by synthesizing the filtered time-domain signal  $u_{RBW}$  using the calculated DM harmonics within the sweeping RBW filter window. Step 2.) was performed by means of an equivalent mathematical representation of the QP detector circuit [24]. Note that the (mostly imperative) distinction between DM and CM noise can easily be done in the frequency-domain of this approach and normally requires extra effort in a simulation.

**Fig. 10(b)** shows the calculated harmonic DM spectrum of the voltages  $u_{pn}$  at the ports {a,b,c} before the filter. Furthermore, the determined QP emission level  $u_{QP}$  is depicted. The Class B limits do not decrease beyond 1 MHz, which is why the critical frequency for the filter design can be identified in **Fig. 10(b)** at  $f_{crit}=158$  kHz. The inspection of the plot reveals a required DM attenuation  $A_{DM}$  of 75 dB at this frequency. Since the shown Class B limits apply to the total DM and CM emissions, a common practice is to increase the required DM attenuation by 6 dB to obtain a margin for the subsequent CM filter design [24]. The resulting filtered spectrum is measured at the interface {L1,L2,L3} between converter and mains by means of a line impedance stabilization network (LISN, [23]). This measurement circuit has an approximate inner resistance of  $R_{LISN} = 50 \Omega$  for frequencies above 150 kHz. The total attenuation of the DM filter and LISN can thus be approximated with

$$\frac{1}{A_{DM}(f)} = \left| \frac{i_p(f)}{u_{pn}(f)} \right| \cdot R_{LISN} \approx \frac{R_{LISN}}{L_{boost} C_{DM} L_{DM} (2\pi f)^3}, \quad (31)$$

if linear filter components are assumed. Using (31) and the component values in **Tab. I**, the desired attenuation

$$A_{DM}(f_{crit} = 158 \text{ kHz}) \approx 1.14 \cdot 10^4 \approx 81.14 \text{ dB}, \quad (32)$$

results. **Fig. 10(c)** shows the calculated attenuated DM spectrum as well as the respective emission levels  $u_{QP}$ . It can be seen that the Class B limits are clearly met with a margin of approximately 11 dB. The discrepancy to the targeted 6 dB is due to the approximation in the filter transfer function (31). The validity and quality of the approach based on the derived formula in this work is proven by the high accuracy when compared to the simulated emission levels. The error is around 2 dB at the upper limit  $m_{max} = 48 \hat{=} 583$  kHz as defined in **Sec. II-F** and reaches only 3 dB at 1 MHz ( $\hat{=} m \approx 82$ ).

## V. CONCLUSION

In this paper, an analytical formula for the approximate calculation of the switching frequency harmonics of idealized PWM-controlled 3-phase 3-level voltage-source DC/AC power converters was presented. The formula is based on the assumption of an infinitely high ratio  $z$  between switching and output fundamental frequency. This assumption is, however, fulfilled to a sufficient degree by most modern converter systems, allowing for accurate calculations of the spectra. An in-depth error analysis has shown that  $z \geq 30$  is sufficient, while good accuracy can be obtained up to high harmonic orders. The simple formula which can be evaluated for almost arbitrary modulation signals is thus an attractive alternative to exact methods, whose demanding derivations yield complex formulas which can mostly be evaluated for a single modulation signal only.

The presented method was further used to derive a universal yet still simple formula for general  $N$ -level converters and again arbitrary modulation signals. Furthermore, it is shown how the effect of non-linear, current-dependent inductors in the output impedance can be incorporated for systems with decoupled phases or, equivalently, single-phase systems.

A design example of an EMI filter demonstrated the usefulness and accuracy of the derived formulas. The MATLAB code presented in the **Appendix** can be used to calculate most of the presented results.

Future work could include a more comprehensive error analysis. Particularly the impact of varying the number of voltage levels  $N$  on the accuracy in general,  $z_{\min}$  and  $m_{\max}$  could be investigated. Finally, more advanced formulas could be derived with the LGI method which incorporate other non-ideal effects besides non-linear inductors. Examples are switching delays, finite switching speeds of the semiconductors and a varying DC-link voltage, which all lead to a distortion of the assumed ideal rectangular voltage pulse trains.

## APPENDIX

MATLAB CODE FOR THE OUTPUT VOLTAGE SPECTRUM OF AN  $N$ -LEVEL CONVERTER

The derived formulas in this work are most suitably implemented in MATLAB using the Symbolic Math Toolbox. This enables a clear and flexible code while benefiting from MATLAB's efficient and accurate numeric methods. Here, the MATLAB code for the generalized  $N$ -level formula (29) is presented.

First the desired modulation function must be defined, such as the flat-top reference,

```
uref = @(M,beta)...
(1.) .* (beta >= 0 & beta <= pi/6) + ...
(-1.+sqrt(3.)).*M.*cos(beta-pi./6)).*...
(beta > pi/6 & beta <= pi/2) + ...
(1.-sqrt(3.)).*M.*cos(-beta+5.*pi./6)).*...
(beta > pi/2 & beta <= 5*pi/6) + ...
(-1.) .* (beta >= 5*pi/6 & beta <= pi);
```

Other modulation signals can be coded analogously. In a next step, the integrand of the  $N$ -level formula (29) and (30) are defined,

```
N_ast = @(N,M,beta)...
1+floor((uref(M,beta)+1)/(2/(N-1)));

int_NLevel = @(UDC,N,m,k,M,beta)...
2.*(1-(-1)^(m+k)).*UDC/((N-1).*m.*pi^2).*...
```

```
cos(k.*beta).*sin(1/2.*m.*pi.*...
(1+N-2.*N_ast(N,M,beta)+(-1+N).*uref(M,beta)));
```

An arbitrary harmonic can now be calculated using MATLAB's `integral()` method,

```
UDC=1000; N=3; m=1; k=0; M=1.;

U_mz_k = integral(@(beta)...
int_NLevel(UDC,N,m,k,M,beta),0,pi/2)
```

## REFERENCES

- [1] M. Odavic, M. Sumner, P. Zanchetta, and J. Clare, "A Theoretical Analysis of the Harmonic Content of PWM Waveforms for Multiple-Frequency Modulators," *IEEE Trans. PE*, vol. 25, no. 1, pp. 131–141, 2010.
- [2] J. T. Boys and P. G. Handley, "Harmonic Analysis of Space Vector Modulated PWM Waveforms," *Proc. IEE*, vol. 137, no. 4, pp. 197–204, 1990.
- [3] R. Guinee and C. Lyden, "A Novel Single Fourier Series Technique for the Simulation and Analysis of Asynchronous Pulse Width Modulation," in *Proc. APEC*, vol. 1, pp. 123–128 vol.1, 1998.
- [4] G. Fedele and D. Frascino, "Spectral Analysis of a Class of DC-AC PWM Inverters by Kapteyn Series," *IEEE Trans. PE*, vol. 25, no. 4, pp. 839–849, 2010.
- [5] D. Kostic, Z. Avramovic, and N. Ciric, "A New Approach to Theoretical Analysis of Harmonic Content of PWM Waveforms of Single- and Multiple-Frequency Modulators," *IEEE Trans. PE*, vol. 28, no. 10, pp. 4557–4567, 2013.
- [6] W. R. Bennett, "New Results in the Calculation of Modulation Products," *Bell System Technical Journal*, vol. 12, no. 2, pp. 228–243, Apr. 1933.
- [7] H. Black, *Modulation Theory*, 1st ed. Van Nostrand Reinhold Company, 1953.
- [8] S. Bowes and B. Bird, "Novel Approach to the Analysis and Synthesis of Modulation Processes in Power Converters," *Proc. IEE*, vol. 122, no. 5, pp. 507–513, 1975.
- [9] S. Bowes, "New Sinusoidal Pulsewidth-Modulated Inverter," *Proc. IEE*, vol. 122, no. 11, pp. 1279–1285, 1975.
- [10] G. Carrara, S. Gardella, M. Marchesoni, R. Salutari, and G. Sciutto, "A New Multilevel PWM Method: A Theoretical Analysis," *IEEE Trans. PE*, vol. 7, no. 3, pp. 497–505, 1992.
- [11] J. F. Moynihan, M. Egan, and J. M. D. Murphy, "Theoretical Spectra of Space-Vector-Modulated Waveforms," *Proc. IEE EPA*, vol. 145, no. 1, pp. 17–24, 1998.
- [12] M. Bierhoff, F. Fuchs, and S. Pischke, "Theoretical Output Current Spectra of Three Phase Current Source Converters," in *Proc. PEA*, pp. 9 pp.–P9, 2005.
- [13] D. G. Holmes and T. A. Lipo, *Pulse Width Modulation for Power Converters*. New York: Wiley, 2003.
- [14] H. van der Broeck, "Analysis of the Voltage Harmonics of PWM Voltage Fed Inverters Using High Switching Frequencies and Different Modulation Functions," *ETEP*, vol. 2, no. 6, pp. 341–350, Nov./Dec. 1992.
- [15] K. Zhou and D. Wang, "Relationship Between Space-Vector Modulation and Three-Phase Carrier-Based PWM: A Comprehensive Analysis," *IEEE Trans. IE*, vol. 49, no. 1, pp. 186–196, 2002.
- [16] *Electromagnetic Compatibility (EMC) – Part 3-12: Limits – Limits for Harmonic Currents Produced by Equipment Connected to Public Low-voltage Systems with Input Current >16 A and ≤75 A per Phase*, IEC 61000-6-4, 2011.
- [17] *Recommended Practices and Requirements for Harmonic Control in Electrical Power Systems*, IEEE 519, 1992.
- [18] *Technical Guideline Generating Plants Connected to the Medium-Voltage Network*, BDEW Std., 2008.
- [19] J. W. Kolar, H. Ertl., and F. C. Zach, "Calculation of the Passive and Active Component Stress of Three-Phase PWM Converter Systems with High Pulse Rate," in *Proc. EPE*, pp. 1303–1311, 1989.
- [20] J. Kolar, H. Ertl, and F. C. Zach, "Influence of the Modulation Method on the Conduction and Switching Losses of a PWM Converter System," *IEEE Trans. IA*, vol. 27, no. 6, pp. 1063–1075, 1991.
- [21] *Electromagnetic Compatibility (EMC) – Part 6-3: Generic Standards – Emission Standard for Residential, Commercial and Light-Industrial Environments*, IEC 61000-6-3, 2006.
- [22] *Electromagnetic Compatibility – Requirements for Household Appliances, Electric Tools and Similar Apparatus*, CISPR 14, 2008.
- [23] *Specification for Radio Disturbance and Immunity Measuring Apparatus and Methods*, CISPR 16, 2010.
- [24] M. L. Heldwein, "EMC Filtering of Three-Phase PWM Converters," Ph.D. dissertation, ETH Zurich, 2007.